ARTICLES
https://doi.org/10.1038/s41567-018-0190-0

nature physics

Corrected: Author Correction

Even-denominator fractional quantum Hall states at an isospin transition in monolayer graphene

A. A. Zibrov[1,4], E. M. Spanton[2,4], H. Zhou[1], C. Kometter[1], T. Taniguchi[3], K. Watanabe[3] and A. F. Young[1*]

In monolayer graphene, the two inequivalent sublattices of carbon atoms combine with the electron spin to give electrons a nearly fourfold degenerate internal isospin. At high magnetic fields, the isospin degeneracy increases the already large intrinsic degeneracy of the two-dimensional Landau levels, making low-disorder graphene systems a versatile platform for studying multicomponent quantum magnetism. Here, we describe magnetocapacitance experiments of ultraclean monolayer graphene devices in which a hexagonal boron nitride substrate breaks the symmetry between carbon sublattices. We observe a phase transition in the isospin system, which is marked by unusual transitions in odd-denominator fractional quantum Hall states for filling factors ν near charge neutrality and by the unexpected appearance of incompressible even-denominator fractional quantum Hall states at $\nu=\pm1/2$ and $\nu=\pm1/4$. We propose a scenario in which the observed states are multicomponent fractional quantum Hall states incorporating correlations between electrons on different carbon sublattices, associated with a quantum Hall analogue of the Néel-to-valence bond solid transition that occurs at charge neutrality.

Clean two-dimensional electron systems in the high-magnetic-field limit host various correlated phenomena, including Wigner crystallization of electrons, topologically ordered fractional quantum Hall liquids, and quantum Hall ferromagnets. Among such systems, monolayer graphene is distinguished by its zero-energy Landau level (ZLL), which spans $\nu\in[-2,2]$ with $\nu\equiv 2\pi\ell_B^2 n_e$ the Landau level filling factor. Here, n_e is the areal electron density and $\ell_B^2=\hbar/eB$ is the magnetic length. The fourfold degeneracy of the ZLL reflects the near-degeneracy of internal spin and sublattice quantum numbers, while the π-Berry phase of the massless Dirac electrons pins the centre of the ZLL to charge neutrality at $n_e=0$. Within the ZLL, the dominant long-ranged Coulomb interaction does not distinguish between different spin or sublattice flavours, but favours breaking the approximate SU(4) isospin symmetry by polarizing the ground state into a single isospin component[1]. Broken isospin symmetry manifests principally as additional gapped states[2,3] at integer fillings $\nu=0,\pm1$.

Of particular interest is the case of the charge neutral state at $\nu=0$, corresponding to half-filling of the ZLL, where Pauli exclusion prevents, for example, simultaneous spin and sublattice polarization. In this case, the direction of polarization is set by competing isospin anisotropies, including both single-particle effects and the anisotropy of the Coulomb interactions at the scale of the honeycomb lattice. Candidate $\nu=0$ ground states are sketched in Fig. 1a and characterized by either spin or sublattice order, including a canted antiferromagnetic (CAF) state that breaks spin rotation symmetry[4] and a partially sublattice polarized (PSP) density wave featuring a Kekulé distortion that triples the size of the unit cell[5].

The CAF and PSP states are direct analogs of the Néel and valence bond solid (VBS) states that arise in studies of two-dimensional quantum magnetism, as noted in a series of recent theoretical works[6–8]. Within conventional Landau–Ginzburg–Wilson theory, incompatible symmetry breaking between the VBS and Néel phases (real-space and spin, respectively) requires a first-order transition. However, unusual critical phases allowing for a continuous transition have been proposed[9], as well as first-order transitions with emergent symmetry at the critical point[7]. Realizing the PSP–CAF transition in monolayer graphene could thus allow direct experimental probes of this unconventional quantum phase transition.

Here we report the observation of anomalous fractional quantum Hall features at low $|\nu|$, consistent with proximity to a PSP–CAF phase transition at $\nu=0$. The transition is marked by the appearance—and subsequent disappearance—of even-denominator fractional quantum Hall (EDFQH) states at $\nu=\pm1/2$ and $\nu=\pm1/4$ in the vicinity of charge neutrality, coincident in magnetic field with weakening of nearby odd-denominator fractional quantum Hall (ODFQH) states across the range $-2/3<\nu<2/3$. We observe a similar phenomenology in three monolayer graphene samples (A, B and C) fabricated by encapsulating the graphene flake between single-crystal hexagonal boron nitride gate dielectrics and single-crystal graphite electrostatic gates[10,11]. The magnetic field at which the anomalous FQH features are observed is directly correlated with the strength of an observed zero-field insulating state associated with a substrate-induced sublattice splitting Δ_{AB}, with the $\nu=\pm1/2$ states appearing for a narrow range of magnetic field centred on 28.3 T, 27.5 T and 5.6 T in the three devices. We interpret the observed features within a model in which a magnetic field-dependent antiferromagnetic interaction anisotropy[12] competes with a fixed substrate-induced sublattice-symmetry-breaking gap[13,14], leading to a transition between sublattice- and spin-ordered phases at both neutrality[15,16] and nearby fractional fillings[17].

Figure 1b shows the penetration field capacitance (C_P) for sample A, where C_P is defined as the differential capacitance between the top and bottom gates with the graphene held at constant electrochemical potential[18]. Data are plotted over a range spanning the ZLL as a function of magnetic field B and nominal charge carrier density $n_0=c(v_t+v_b-2v_s)$, where c is the average gate-to-sample geometric capacitance of the two (nearly symmetric) gates and v_t, v_b

[1]Department of Physics, University of California, Santa Barbara, CA, USA. [2]California Nanosystems Institute, University of California at Santa Barbara, Santa Barbara, CA, USA. [3]Advanced Materials Laboratory, National Institute for Materials Science, Tsukuba, Japan. [4]These authors contributed equally: A. A. Zibrov, E. M. Spanton. *e-mail: andrea@physics.ucsb.edu

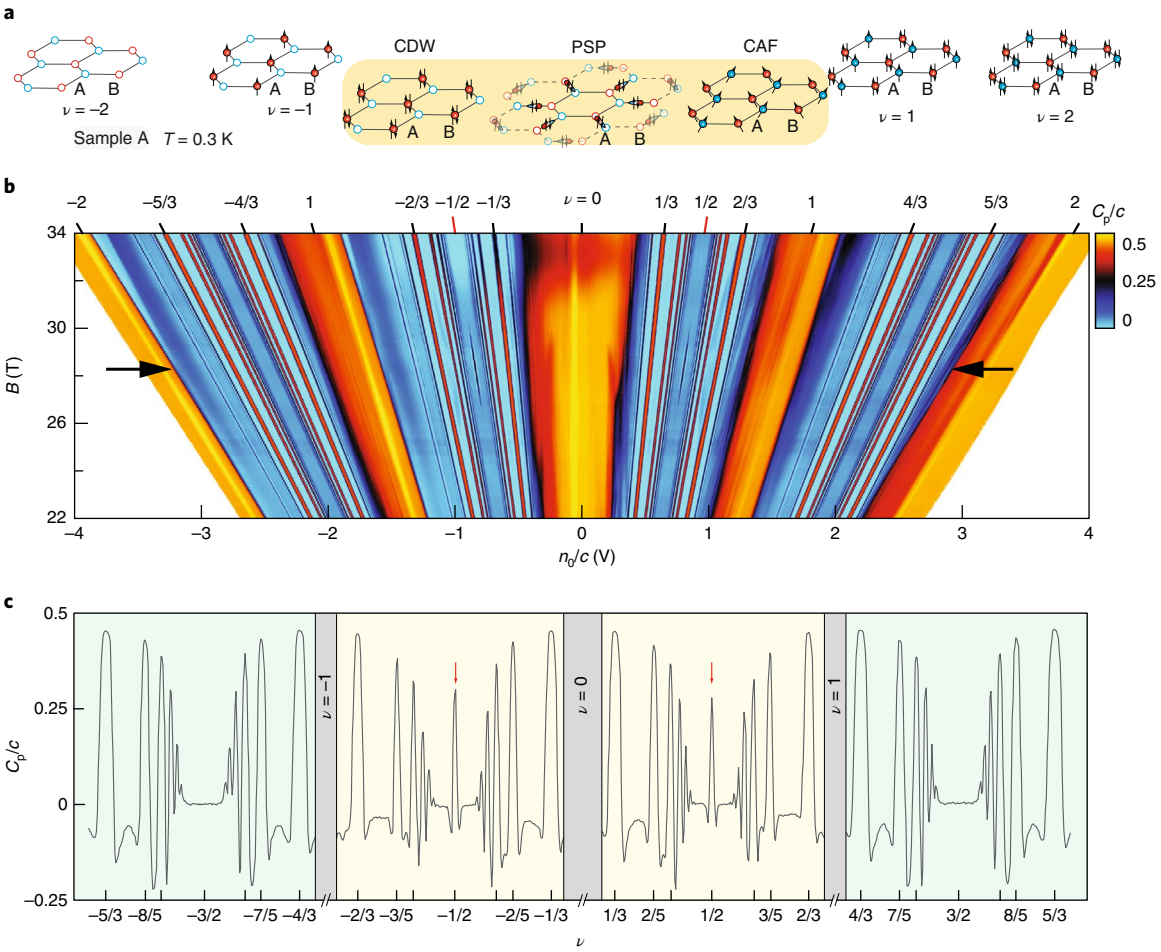

Fig. 1 | Incompressible FQH states at $\nu = \pm 1/2$. a, Sketches of ground state spin and sublattice polarizations at integer filling within the ZLL. At $\nu = -2$ the ZLL is empty while at $\nu = +2$ it is fully filled. At $\nu = \pm 1$, single or triple occupation permits full spin and sublattice polarization. At $\nu = 0$, however, corresponding to half filling, a variety of ground states are predicted[4,5,15,16,45], including charge density wave (CDW), partially sublattice polarized (PSP) and canted antiferromagnetic (CAF) phases. **b**, False-colour plot of the penetration field capacitance C_p/c measured (see Methods) in sample A at $T = 300$ mK as a function of the magnetic field, B, and the nominal charge density $n_0 \equiv c(v_t + v_b - 2v_s)$, where v_t, v_b and v_s are the top gate, bottom gate and sample voltages, respectively. c is the average geometric capacitance of the two gates. Fractional quantum Hall states appear as lines of high C_p with a slope proportional to their quantized Hall conductivity[19]. The dataset spans filling factors $\nu = [-2,2]$, encompassing the zero-energy Landau level. **b**, C_p trace taken at constant $B = 28.3$ T between filling factors $\nu = -2$ and $\nu = 2$, corresponding to the black arrows in **a**. Incompressible states occur at $\nu = \pm 1/2$ (red arrows), indicating an even-denominator fractional quantum Hall state, while $\nu = \pm 3/2$, which are farther away from charge neutrality, remain compressible. Incompressible features associated with the integer quantum Hall states are omitted to more clearly show the FQH features.

and v_s are the voltages applied to top gate, bottom gate and sample, respectively. We observe gapped quantum Hall states, which appear as peaks in the measured signal at constant ν (see Methods), at integer fillings $\nu = \pm 2$, ± 1 and 0, as well as at fractional filling factors $|\nu - \lfloor \nu \rfloor| = \frac{p}{mp \pm 1}$, where $\lfloor \nu \rfloor$ is the greatest integer less than or equal to ν. We observe states with $m = 2,4$ and p large as 7 (Fig. 1a,b and Supplementary Fig. 1). In the absence of four-terminal measurements we extract the Hall conductivity of the high-C_p gapped states using the Středa formula[19], which states that gaps following a linear trajectory in the density–magnetic field plane carry quantized Hall conductivity equivalent to their slope.

Incompressible EDFQH states appear at $\nu = \pm 1/2$, but only in a narrow range of magnetic fields. Similar phenomenology is also observed at $\nu = \pm 1/4$, with EDFQH appearing only for a small range of B (Fig. 2 and Supplementary Fig. 1). The appearance of EDFQH states is accompanied by weakening or disappearance of adjacent ODFQH states. This is evident both near $\pm 1/4$ (Fig. 2) and $\pm 1/2$ (Fig. 3a,c and Supplementary Figs. 2 and 4), with weakening most evident at temperatures comparable to the ODFQH energy gaps (see Supplementary Fig. 14). In sample C, an EDFQH state at $\nu = \pm 1/2$ and weakening/disappearance of nearby ODFQH states also occur, but at much lower B (Fig. 3b,d). Both the appearance of the EDFQH states and the weakening of the ODFQH states occur only for fillings near charge neutrality, $\nu \in [-2/3, 2/3]$; for example, no EDFQH is observed at $\nu = \pm 3/4$, $\pm 5/4$, $\pm 3/2$ or $\pm 7/4$ throughout the experimental range of B. The magnetic field for both ODFQH weakening and EDFQH emergence occurs at lower fields for transitions closer to $\nu = 0$, but remains constant for $2/3 > |\nu| > 1/2$ (Fig. 3e,f).

EDFQH states have not been previously reported among the many FQH states observed in monolayer graphene[20–25], nor have they been predicted[26–33]. However, previous experiments on other quantum Hall systems have revealed a variety of behaviours at even-denominator fractional filling. In single-layer semiconductor quantum wells, the two-dimensional electron system is compressible at filling factors $\nu = 1/2$ and $3/2$ in the lowest Landau level (corresponding to orbital quantum number $N = 0$) but forms incompressible FQH states at $\nu = 5/2$ and $7/2$ in the first excited LL (orbital quantum number $N = 1$)[34]. Other single-component FQH

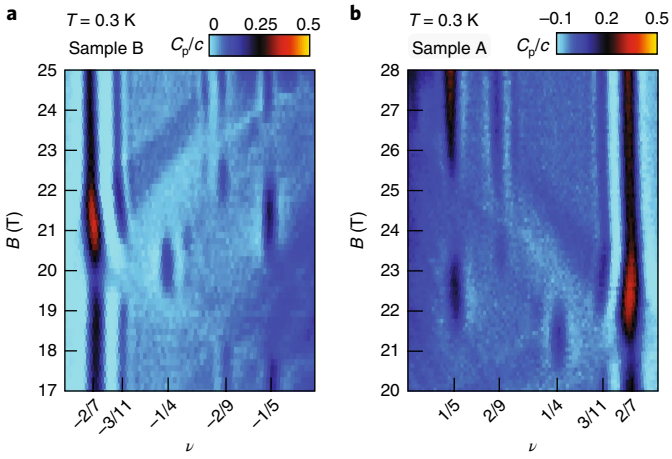

Fig. 2 | Incompressible FQH states at $\nu = \pm 1/4$. a, False-colour plot of C_p/c in sample B as a function of ν and B at T = 300 mK. In addition to the $\nu = -1/4$ state, FQH states from the $\nu = \frac{p}{4p+1}$ ODFQH sequence are visible, with B-dependent weakening associated with isospin phase transitions. **b**, Similar data from sample A near $\nu = +1/4$.

systems, including ZnO[35] and bilayer graphene[10,11,36], show EDFQH at different ν but always in a regime corresponding to occupation of $N = 1$ orbital wavefunctions. In the monolayer graphene ZLL, orbital wavefunctions are identical to the $N = 0$ LL of conventional semiconductor systems, and so no single-component EDFQH states are anticipated[26,27,32,33,37]. Multicomponent systems, however, can host a wider variety of FQH states[38], including at even-denominator filling factors. Indeed, EDFQH states at $\nu = 1/2$[39–42] and $\nu = 1/4$[43,44] have been observed in the $N = 0$ LL for structures where electrons are confined to two spatially separated layers or electronic subbands. By analogy with such systems, it seems likely that the monolayer graphene EDFQH states are multicomponent in nature, with the role of the layer/subband quantum number replaced by isospin components within the ZLL. In this scenario, the ODFHQ weakening is similarly associated with transitions between ODFQH states constructed from different isospin components[24].

The high symmetry of the ZLL permits many possible isospin polarizations at fractional filling, complicating the task of determining the components relevant for forming multicomponent FQH states. However, recent theoretical work has suggested that the isospin phase diagram of low-$|\nu|$ FQH states closely mimics that of the nearby $\nu = 0$ integer quantum Hall state[17], which can be analysed within a Hartree–Fock framework[15,16]. The $\nu = 0$ ground state is obtained by optimizing the energy of competing isospin anisotropies constrained by the Pauli exclusion principle, which prohibits double occupation of a spin or valley component. These anisotropies include the Zeeman effect (with characteristic energy $E_Z = g\mu_B B \approx 1.34\text{K} \times B$ [tesla], where $g = 2$ and μ_B are the g-factor of the electron and the Bohr magneton, respectively), the intrinsic sublattice-anisotropy of the Coulomb interactions themselves[45] (with characteristic energy $E_V = \frac{a}{\ell_B}\frac{e^2}{\varepsilon\ell_B} \approx .98\text{K} \times B[\text{tesla}]$) and substrate-induced sublattice splitting (with characteristic energy Δ_{AB}).

A clue to the origin of the observed FQH features is provided by the observation that all the devices showing EDFQH states and ODFQH features are gapped at zero magnetic field and zero charge density—a phenomenology associated with finite Δ_{AB}. Figure 4a,b shows low-magnetic-field Landau fan plots for samples A and C. The electron system remains incompressible at $\nu = 0$ for all magnetic fields, consistent with a single-particle Δ_{AB} (refs [13,14]). The insulating nature of samples B and C is confirmed by transport measurements at zero field (Supplementary Fig. 8; sample A did not have transport contacts). In a fourth sample showing no measurable sublattice gap, no EDFQH states were observed (Supplementary Figs. 9,10). Crucially, the magnetic field at which EDFQH states appear is directly correlated with the measured Δ_{AB} (see Fig. 4c and Supplementary Fig. 11), with large Δ_{AB} corresponding to devices with a large appearance field for the FQH features.

A similar correlation between B and Δ_{AB} arises from analysing the phase diagram of the $\nu = 0$ state, where Δ_{AB} controls the magnetic field of isospin transitions. To investigate this connection quantitatively, we analyse a mean-field model for the charge neutral state that accounts for the sublattice symmetry breaking Δ_{AB} observed in our devices. Such a model has already been studied in the literature for bilayer graphene[15], where sublattice splitting can be actuated with an applied electric field, but is equally applicable in the present scenario. Symmetry considerations permit two competing interaction anisotropies, parameterized by dimensionless couplings g_z and $g_\perp$ which we take to be Δ_{AB}- and B-independent constants. The resulting phase diagram[15,16] includes both the PSP and CAF phases mentioned above as well as a fully sublattice polarized charge density wave (CDW) state and fully spin polarized ferromagnetic (FM) state.

Among the competing isospin anisotropies, both E_V and E_Z grow with B while Δ_{AB} is independent of B. Thus the CDW phase is favoured in the low-B limit for $\Delta_{AB} \neq 0$, with phase transitions to E_V- or E_Z-driven states possible at higher B. The values of g_z and $g_\perp$ are constrained to $g_\perp \approx -10$ and $g_z > -g_\perp$ from previous experiments[2,12] on devices with $\Delta_{AB} = 0$ (see Supplementary Information). Figure 4d shows the calculated phase diagram as a function of Δ_{AB} and B for fixed $g_\perp = -10$ and $g_z = 15$. Two phase transitions are evident within this model: a second-order transition from the CDW to PSP phase, corresponding to the canting of the sublattice order parameter into the plane, and a first-order transition from the PSP to CAF phase.

Associating the EDFQH states with a particular phase or phase transition of the $\nu = 0$ ground state imposes two requirements. First, effective interactions and available components at $\nu = \pm 1/2$ (and $\pm 1/4$) should favour formation of an incompressible state. Second, these favourable conditions should persist only for a narrow range of magnetic fields. We propose that these requirements can be satisfied at the PSP–CAF phase transition. In this scenario, EDFQH states are made up of two isospin components with opposite sublattice occupation, which become degenerate in energy near the transition, thus favouring multicomponent states. Furthermore, the anisotropy of Coulomb interactions between wavefunctions on different sublattices is reminiscent of double-layer systems, where asymmetry between inter- and intralayer interactions leads to the formation of a multicomponent EDFQH state[38–40]. The PSP–CAF phase transition also provides a mechanism for the concomitant weakening of ODFQH states, which are predicted to undergo isospin transitions[17]. We note that some other experimental systems have been successfully described using a picture of Zeeman-driven transitions of non-interacting composite fermion LLs[24,35,46]. However, such a naive picture fails to explain a number of qualitative features of our data, most notably the observed weakening of ODFQH states at $\nu = \pm 1/3, \pm 1/5$. It thus appears empirically necessary to consider the full range of multicomponent FQH states allowed in the ZLL to qualitatively understand the FQH physics[17,47].

We illustrate the mechanism for forming a multi-component incompressible state at the CAF–PSP phase transition by ignoring both the canting of spin in the CAF phase (making it a collinear antiferromagnet, denoted AF) and canting of sublattice polarization in the PSP (making it equivalent to the CDW). In this limit, the CDW–AF phase transition is direct, with increasing magnetic field leading to a level crossing between single-electron LLs with identical spin but opposite sublattice polarizations, depicted schematically in Fig. 5. On both sides of the transition, the $\nu = -1$ state is fully spin and sublattice polarized. Additional electrons, however,

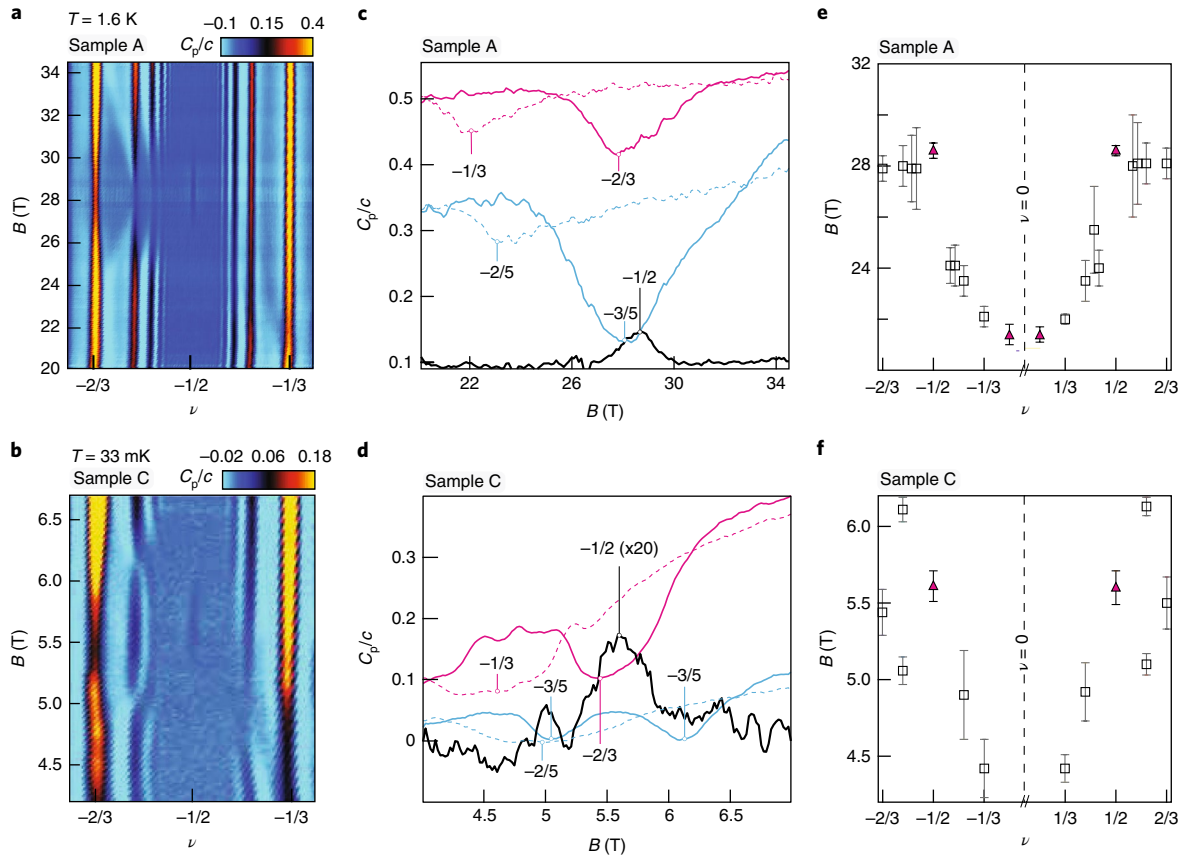

Fig. 3 | Odd-denominator fractional quantum Hall phase transitions associated with the $\nu = -1/2$ state. a, C_p as a function of B and ν in the vicinity of $\nu = -1/2$ state for sample A, taken at $T = 1.6$ K near $B = 28$ T. **b**, Similar data from Sample C, taken at $T = 33$ mK for B near 5.6 T. **c**,**d**, C_p peak height for selected FQH states $\nu \in (-1,0)$, plotted as a function of B, for sample A (**c**) and sample C (**d**), showing the simultaneous strengthening of the even-denominator state and weakening of adjacent odd-denominator states. **e**, Positions of minima (maxima) of the odd (even)-denominator FQH states for $\nu \in (-1,1)$ in Sample A at $T = 1.6$ K. **f**, Similar analysis of sample C at $T = 33$ mK. In sample C, two gap closings are observed at $\nu = \pm 3/5$, whereas only one single gap weakening is observed in sample A. Error bars in **e** and **f** are defined as the range of magnetic fields where the dips (peaks) are within 10% of their extremal value relative to a smooth background.

populate different sublattice orbitals in the low- and high-B regimes: in the CDW, electrons populate the same sublattice, while in the AF regime they populate the opposite sublattice. Far from the transition, additional electrons occupy the lower-energy sublattice branch of the LL, resulting in a compressible state as observed in experiment. Near the transition, however, the two sublattice orbitals are degenerate, making inter-sublattice correlated states---which reduce the energy cost of Coulomb repulsion---energetically favourable. We interpret EDFQH at $\nu = \pm 1/2$ and $\nu = \pm 1/4$ as multicomponent states[38] incorporating intersublattice correlations. We note, however, that within this class of states a variety of multicomponent wavefunctions are possible[17]. Definitive resolution of the nature of the EDFQH will thus require more detailed numerical and experimental studies.

A number of experimental observations, however, are not explained even qualitatively in the simple picture described above, and warrant further study. For example, the counting of ODFQH phases is not well understood: the presence of three phases at $\nu = 1/5$ (Fig. 2), and differences in the number of phases observed at $\nu = \pm 3/5$ for samples with differing Δ_{AB} (Fig. 3a,b), suggest a complex interplay of symmetry breaking and FQH physics. The nature of the transitions between ODFQH states are also open to further investigation. Some filling factors show a full closing of the gap (Fig. 2), while others exhibit only a weakening (for example, Fig. 3a). Finally, the ν dependence of the value of B at which anomalous FQH features appear is strongly dependent on ν for $|\nu| < 1/2$ but appears to completely flatten when $|\nu| > 1/2$ (Fig. 3e,f), a phenomenon that must be accounted for quantitatively in any definitive description of the FQH transitions.

In summary, we have reported the observation of a number of sublattice-splitting tuned FQH phase transitions in monolayer graphene, as well as the observation of EDFQH states at $\nu = \pm 1/2$ and $\pm 1/4$. Athough existing theoretical work has pointed out the possibility of new filling-factor-dependent isospin phases[17,48] arising from the interplay of symmetry breaking and FQH physics, the EDFQH was not predicted and remains to be definitively explained. We expect that future theoretical and experimental work—for example, measurements of tunnelling exponents of EDFQH edge states—will be able to resolve the nature of these new phases.

In addition to the obvious puzzle concerning the precise nature of the FQH states, our analysis suggests the possible existence of previously unexplored isospin phase transitions at $\nu = 0$. The PSP–CAF transition, in particular, remains the subject of continued study. Some authors have proposed that quantum fluctuations destroy the first-order phase transition, leading to a deconfined critical point between the two phases[6,8], while others suggest the first-order phase transition survives but with an enlarged symmetry of low-energy isospin rotations[7]. The most spectacular experimental manifestations of these transitions are likely to occur in the neutral sector, to which the current experiment is blind. However, future experiments

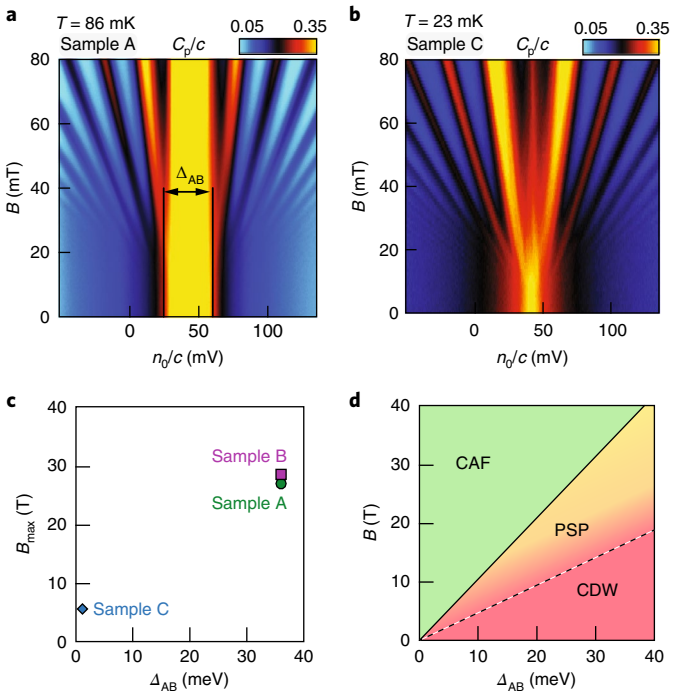

Fig. 4 | Low-*B* data and mean field phase diagram of the $\nu = 0$ state. **a**, Low-field Landau fan in sample A, showing evidence of a large zero-field gap Δ_{AB} induced by sublattice splitting. **b**, Similar data for sample C, showing a much smaller sublattice gap. **c**, The estimated gap sizes for the three measured samples (Δ_{AB} plotted against the magnetic field at which the $\nu = \pm 1/2$ states are maximal (B_{max}). **d**, Calculated phase diagram at $\nu = 0$ for monolayer graphene as a function of magnetic field B and sublattice splitting Δ_{AB}. The stability of the canted antiferromagnet (CAF), a sublattice polarized charge density wave (CDW), and a valley-coherent partially sublattice polarized phase (PSP) were calculated using anisotropy parameters $g_\perp = -10$ and $g_z = 15$ (ref. [16]) (see Supplementary Figs. 17 and 18 and the associated discussion in the Supplementary Information).

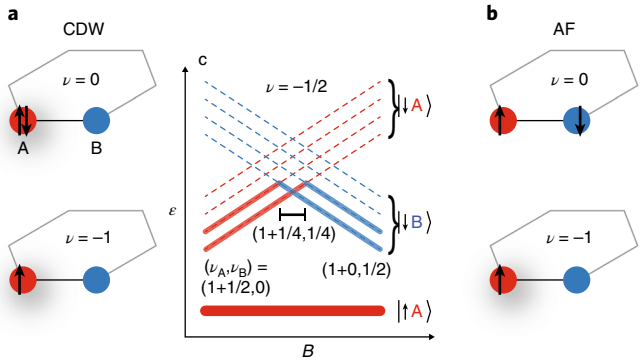

Fig. 5 | Sublattice level crossing and multicomponent $\nu = \pm 1/2$ states within a simplified model. **a**, Spin and sublattice polarizations of $\nu = -1$ and $\nu = 0$ integer quantum Hall ferromagnetic states in the low-B regime where the charge neutral ground state is in the CDW phase. **b**, Spin and sublattice polarizations of $\nu = -1$ and $\nu = 0$ integer quantum Hall ferromagnetic states in the high-B regime. Within this model, which neglects spin canting, the charge neutral ground state is a collinear antiferromagnet (AF). **c**, Level crossing at $\nu = -1/2$ (an identical scenario is obtained at $\nu = +1/2$ by particle-hole conjugation across the ZLL). The $\nu = -1$ state is identical in both cases, consisting of a single fully sublattice- and spin-polarized LL, denoted $|\uparrow A\rangle$. On the CDW side of the transition, $\nu = -1/2$ consists of an additional partially filled $|\downarrow A\rangle$ LL, while in the AF the opposite sublattice is filled, $|\downarrow B\rangle$; both cases result in compressible behaviour. When the two levels are nearly degenerate, Coulomb interactions can favour a multicomponent state with equal sublattice occupation $(\nu_A,\nu_B) = (1+1/4, 1/4)$. Bold lines indicate filled levels: the $|\downarrow A\rangle$ and $|\downarrow B\rangle$ levels are pictured as four branches to depict partial occupation.

can access this physics directly—for instance, by probing thermal[49] or magnetic[50] transport.

Methods

We used the van der Waals dry transfer method to assemble graphite/hBN/MLG/hBN/graphite heterostructures, where hBN is hexagonal boron nitride and MLG is monolayer graphene. Graphite contact(s) were incorporated in the stack to contact the dual-gated monolayer. hBN thicknesses of 40–60 nm were used, while graphite contacts and gates were between 3 nm and 10 nm thick. In samples A–C, windows to the graphite contacts and gates were etched in a Xetch-X3 xenon difluoride etching system, a selective hBN etch, and defluorinated with a 400 °C anneal in the forming gas. The gates and contacts were then contacted Ti/Au (5 nm/100 nm) contacts. In sample D, edge contacts[51] to the graphite were made with Cr/Pd/Au (3 nm/15 nm/80 nm). Optical images of the four measured devices are shown in Supplementary Fig. 16 Measurements below $B = 14$ T were performed in a top-loading Bluefors dry dilution refrigerator. Reported temperatures were measured using a ruthenium oxide thermometer attached to the cold finger. Measurements at higher magnetic field were performed at the National High Magnetic Field Lab in Tallahassee in a 35 T resistive magnet and 45 T hybrid magnet, in He-3 fridges with a nominal base temperature of 0.3 K. We performed measurements of the penetration field capacitance (C_P) as a function of magnetic field and gate voltages to probe incompressible/insulating states. This measurement technique is outlined in Supplementary Fig. 15 and described in detail in ref. [10] and references therein. Unless otherwise noted, measurements were performed above the low-frequency limit (at $f = 60$–100 kHz)—that is, there is an out-of-phase dissipative signal associated with many of the observed gapped states. In this frequency regime, an elevated C_P indicates a combination of incompressibility and bulk insulating behaviour, both of which are an indication of gapped states[52]. We focus on gapped states at fixed filling factor, which, by arguments first proven by Středa[19], have a quantized Hall conductance equal to their slope in the n–B plane.

In. Fig. 2a, a fixed filling factor running average of three pixels was used to remove line noise which obscured some weaker features. In Fig. 3c,d, a fixed filling factor running average of five pixels was used to remove line noise.

Data availability. The data that support the findings of this study are available from the corresponding author upon reasonable request.

Methods

Methods, including statements of data availability and any associated accession codes and references, are available at https://doi.org/10.1038/s41567-018-0190-0.

Received: 29 November 2017; Accepted: 21 May 2018;
Published online: 2 July 2018

References

1. Nomura, K. & MacDonald, A. H. Quantum Hall ferromagnetism in graphene. *Phys. Rev. Lett.* **96**, 256602 (2006).
2. Checkelsky, J. G., Li, L. & Ong, N. P. Zero-energy state in graphene in a high magnetic field. *Phys. Rev. Lett.* **100**, 206801 (2008).
3. Zhang, Y. et al. Landau-level splitting in graphene in high magnetic fields. *Phys. Rev. Lett.* **96**, 136806 (2006).
4. Herbut, I. F. Theory of integer quantum Hall effect in graphene. *Phys. Rev. B* **75**, 165411 (2007).

5. Nomura, K., Ryu, S. & Lee, D.-H. Field-induced Kosterlitz–Thouless transition in the $N=0$ Landau level of graphene. *Phys. Rev. Lett.* **103**, 216801 (2009).
6. Lee, J. & Sachdev, S. Deconfined criticality in bilayer graphene. *Phys. Rev. B* **90**, 195427 (2014).
7. Wu, F., Sodemann, I., Araki, Y., MacDonald, A. H. & Jolicoeur, T. SO(5) symmetry in the quantum Hall effect in graphene. *Phys. Rev. B* **90**, 235432 (2014).
8. Lee, J. & Sachdev, S. Wess–Zumino–Witten terms in graphene Landau levels. *Phys. Rev. Lett.* **114**, 226801 (2015).
9. Senthil, T., Vishwanath, A., Balents, L., Sachdev, S. & Fisher, M. P. A. Deconfined quantum critical points. *Science* **303**, 1490–1494 (2004).
10. Zibrov, A. A. et al. Tunable interacting composite fermion phases in a half-filled bilayer-graphene Landau level. *Nature* **549**, 360–364 (2017).
11. Li, J. I. A. et al. Even denominator fractional quantum Hall states in bilayer graphene. *Science* **358**, 648–652 (2017).
12. Young, A. F. et al. Tunable symmetry breaking and helical edge transport in a graphene quantum spin Hall state. *Nature* **505**, 528–532 (2014).
13. Hunt, B. et al. Massive Dirac fermions and Hofstadter butterfly in a van der Waals heterostructure. *Science* **340**, 1427–1430 (2013).
14. Amet, F., Williams, J. R., Watanabe, K., Taniguchi, T. & Goldhaber-Gordon, D. Insulating behavior at the neutrality point in single-layer graphene. *Phys. Rev. Lett.* **110**, 216601 (2013).
15. Kharitonov, M. Phase diagram for the ν=0 quantum Hall state in monolayer graphene. *Phys. Rev. B* **85**, 155439 (2012).
16. Kharitonov, M. Canted antiferromagnetic phase of the $\nu=0$ quantum Hall state in bilayer graphene. *Phys. Rev. Lett.* **109**, 046803 (2012).
17. Sodemann, I. & MacDonald, A. H. Broken SU(4) symmetry and the fractional quantum Hall effect in graphene. *Phys. Rev. Lett.* **112,** 126804 (2014).
18. Eisenstein, J. P., Pfeiffer, L. N. & West, K. W. Negative compressibility of interacting two-dimensional electron and quasiparticle gases. *Phys. Rev. Lett.* **68**, 674–677 (1992).
19. Streda, P. Quantised Hall effect in a two-dimensional periodic potential. *J. Phys. C* **15**, L1299–L1303 (1982).
20. Bolotin, K. I. et al. Ultrahigh electron mobility in suspended graphene. *Solid State Commun.* **146**, 351–355 (2008).
21. Du, X., Skachko, I., Duerr, F., Luican, A. & Andrei, E. Y. Fractional quantum Hall effect and insulating phase of Dirac electrons in graphene. *Nature* **462**, 192–195 (2009).
22. Dean, C. R. et al. Multicomponent fractional quantum Hall effect in graphene. *Nat. Phys.* **7**, 693–696 (2011).
23. Feldman, B. E., Krauss, B., Smet, J. H. & Yacoby, A. Unconventional sequence of fractional quantum Hall states in suspended graphene. *Science* **337**, 1196–1199 (2012).
24. Feldman, B. E.et al. Fractional quantum Hall phase transitions and four-flux states in graphene. *Phys. Rev. Lett.* **111,** 076802 (2013).
25. Amet, F. et al. Composite fermions and broken symmetries in graphene. *Nat. Commun.* **6**, 5838 (2015).
26. Apalkov, V. M. & Chakraborty, T. Fractional quantum Hall states of Dirac electrons in graphene. *Phys. Rev. Lett.* **97,** 126801 (2006).
27. Tőke, C. & Jain, J. K. Theoretical study of even denominator fractions in graphene: Fermi sea versus paired states of composite fermions. *Phys. Rev. B* **76**, 081403(R) (2007).
28. Toke, C. & Jain., J. K.. SU(4) composite fermions in graphene: fractional quantum Hall states without analog in GaAs. *Phys. Rev. B* **75,** 245440 (2007).
29. Shibata, N. & Nomura, K. Fractional quantum Hall effects in graphene and its bilayer. *J. Phys. Soc. Jpn* **78**, 104708–104715 (2009).
30. Papic, Z., Goerbig, M. O. & Regnault, N. Atypical fractional quantum Hall effect in graphene at filling factor 1/3. *Phys. Rev. Lett.* **105,** 176802 (2010).
31. Toke, C. & Jain, J. K. Multi-component fractional quantum Hall states in graphene: SU(4) versus SU(2). *J. Phys. Condens. Matter* **24**, 235601 (2011).
32. Papic, Z., Thomale, R. & Abanin, D. A. Tunable electron interactions and fractional quantum Hall states in graphene. *Phys. Rev. Lett.* **107,** 176602 (2011).
33. Peterson, M. R. & Nayak, C. Effects of Landau level mixing on the fractional quantum Hall effect in monolayer graphene. *Phys. Rev. Lett.* **113,** 086401 (2014).
34. Willett, R. et al. Observation of an even-denominator quantum number in the fractional quantum Hall effect. *Phys. Rev. Lett.* **59**, 1776–1779 (1987).
35. Falson, J. et al. Even-denominator fractional quantum Hall physics in ZnO. *Nat. Phys.* **11**, 347–351 (2015).
36. Ki, D.-K., Fal'ko, V. I., Abanin, D. A. & Morpurgo, A. F. Observation of even denominator fractional quantum Hall effect in suspended bilayer graphene. *Nano Lett.* **14**, 2135–2139 (2014).
37. Abanin, D. A., Skachko, I., Du, X., Andrei, E. Y. & Levitov, L. S. Fractional quantum Hall effect in suspended graphene: transport coefficients and electron interaction strength. *Phys. Rev. B* **81,** 115410 (2010).
38. Halperin, B. I. Theory of the quantized Hall conductance. *Helv. Phys. Acta* **56**, 75–102 (1983).
39. Suen, Y. W., Engel, L. W., Santos, M. B., Shayegan, M. & Tsui, D. C. Observation of a $\nu=1/2$ fractional quantum Hall state in a double-layer electron system. *Phys. Rev. Lett.* **68**, 1379–1382 (1992).
40. Eisenstein, J. P., Boebinger, G. S., Pfeiffer, L. N., West, K. W. & He, S. New fractional quantum Hall state in double-layer two-dimensional electron systems. *Phys. Rev. Lett.* **68**, 1383–1386 (1992).
41. Liu, Y. et al. Even-denominator fractional quantum Hall effect at a Landau level crossing. *Phys. Rev. B* **89**, 165313 (2014).
42. Liu, Y. et al. Fractional quantum Hall effect at $\nu=1/2$ in hole systems confined to GaAs quantum wells. *Phys. Rev. Lett.* **112**, 046804 (2014).
43. Luhman, D. R. et al. Observation of a fractional quantum Hall state at $\nu=1/4$ in a wide GaAs quantum well. *Phys. Rev. Lett.* **101**, 266804 (2008).
44. Shabani, J., Gokmen, T., Chiu, Y. T. & Shayegan, M. Evidence for developing fractional quantum Hall states at even denominator 1/2 and 1/4 fillings in asymmetric wide quantum wells. *Phys. Rev. Lett.* **103**, 256802 (2009).
45. Alicea, J. & Fisher, M. P. A. Graphene integer quantum Hall effect in the ferromagnetic and paramagnetic regimes. *Phys. Rev. B* **74**, 075422 (2006).
46. Du, R. R. et al. Fractional quantum Hall effect around v=3/2: composite fermions with a spin. *Phys. Rev. Lett.* **75**, 3926–3929 (1995).
47. Balram, A. C., Toke, C., Wojs, A. & Jain, J. K. Phase diagram of fractional quantum Hall effect of composite fermions in multicomponent systems. *Phys. Rev. B* **91**, 045109 (2015).
48. Abanin, D. A., Feldman, B. E., Yacoby, A. & Halperin, B. I. Fractional and integer quantum Hall effects in the zeroth Landau level in graphene. *Phys. Rev. B* **88**, 115407 (2013).
49. Pientka, F., Waissman, J., Kim, P. & Halperin, B. I. Thermal transport signatures of broken-symmetry phases in graphene. *Phys. Rev. Lett.* **119**, 027601 (2017).
50. Wei, Di. S. et al. Electrical generation and detection of spin waves in a quantum Hall ferromagnet. Preprint at http://arXiv.org/abs/1801.08534 (2018).
51. Wang, L. et al. One-dimensional electrical contact to a two-dimensional material. *Science* **342**, 614–617 (2013).
52. Goodall, R. K., Higgins, R. J. & Harrang, J. P. Capacitance measurements of a quantized two-dimensional electron gas in the regime of the quantum Hall effect. *Phys. Rev. B* **31**, 6597–6608 (1985).

Acknowledgements

We acknowledge discussions with D. Abanin, G. Murthy, Z. Papic, I. Sodemann and M. Zaletel and the experimental assistance of S. Hannahs. Magnetocapacitance measurements were funded by the National Science Foundation under DMR-1654186. A portion of the nanofabrication and transport measurements were funded by Army Research Office under proposal 69188PHH. A.F.Y. acknowledges the support of the David and Lucile Packard Foundation. E.M.S. acknowledges the support of the Elings Prize Fellowship in Science of the California Nanosystems Institute at the University of California, Santa Barbara (UCSB). The research reported here made use of shared facilities of the UCSB Materials Research Science and Engineering Center (NSF DMR 1720256), a member of the Materials Research Facilities Network (www.mrfn.org). Measurements above 14 T were performed at the National High Magnetic Field Laboratory, which is supported by National Science Foundation Cooperative agreement no. DMR-1157490 and the State of Florida. K.W. and T.T. acknowledge support from the Elemental Strategy Initiative conducted by the Ministry of Education, Culture, Sports, Science and Technology, Japan, and the Japan Society for the Promotion of Science KAKENHI grant no. JP15K21722.

Author contributions

E.M.S. fabricated devices A, B and C, and H.Z. fabricated device D.T.T. and K.W. synthesized the hexagonal boron nitride crystals. A.F.Y. and C.K. built the measurement electronics. A.A.Z., E.M.S. and A.F.Y. acquired and analysed the experimental data. A.A.Z., E.M.S. and A.F.Y. wrote the paper.

Competing interests

The authors declare no competing interests.

Additional information

Supplementary information is available for this paper at https://doi.org/10.1038/s41567-018-0190-0.

Reprints and permissions information is available at www.nature.com/reprints.

Correspondence and requests for materials should be addressed to A.F.Y.

Publisher's note: Springer Nature remains neutral with regard to jurisdictional claims in published maps and institutional affiliations.